Received: 8 February 2018 | Revised: 9 March 2019 | Accepted: 15 March 2019

DOI: 10.1002/joc.6079

RESEARCH ARTICLE

International Journal of Climatology RMetS

Uncertainty in climate projections and time of emergence of climate signals in the western Canadian Prairies

Elaine M. Barrow | **David J. Sauchyn**

Prairie Adaptation Research Collaborative (PARC), University of Regina, Regina, Canada

Correspondence
Elaine M. Barrow, Prairie Adaptation Research Collaborative (PARC), University of Regina, 3737 Wascana Parkway, Regina, Saskatchewan, S4S 0A2, Canada.
Email: elaine.barrow@sasktel.net

Funding information
Climate Research Branch of Environment and Climate Change Canada

This paper has examined the relative significance of uncertainty in future climate projections from a subset of the coupled model intercomparison project phase 5 (CMIP5) global climate models for the Prairie Provinces of western Canada. This was undertaken by determining: (a) the contribution of model and scenario uncertainty and natural variability to the total variance of these future projections, and (b) the timing of climate signal emergence from the background noise of natural climate variability. We examined future projections of mean temperature, precipitation and summer climate moisture index (CMI). In this region, natural climate variability plays an important role in future uncertainty until the end of this century, particularly for precipitation and to a lesser extent, summer CMI. Model uncertainty also contributes to total uncertainty for these variables throughout this century, while scenario uncertainty becomes more important towards the end of the century. For the region as a whole, significant climate change (i.e., signal/noise >2) occurs earliest for summer mean temperature, with median time of emergence around 2035 for the RCP8.5 radiative forcing scenario. Although the median precipitation signal emerges from the noise (i.e., signal/noise >1) around the 2070s in winter and the 2080s in spring, significant values do not occur in any season for this variable before 2100. For summer CMI, the median time of emergence for significant change is around 2085. At the grid scale, signal-to-noise ratios are significant for all seasons for mean surface air temperature, with earliest times of emergence occurring in summer. In contrast, the summer precipitation signal is not significant this century; for summer CMI, significant values are obtained in the eastern half of the region, occurring from about 2065 onwards. Median times of emergence are towards the end of the century for summer CMI in western Saskatchewan and in Alberta, although some areas of Alberta do not exhibit significant signals this century.

KEYWORDS
CMIP5, natural variability, time of emergence, uncertainty, variance partitioning

1 | INTRODUCTION

Numerical climate models are "the primary tools available for investigating the response of the climate system to various forcings, for making climate predictions on seasonal to decadal time scales and for making projections of future climate over the coming century and beyond" (Flato et al., 2013). Applied properly, the climate change scenarios derived from these models are the most rigorous scientific basis for climate change impact assessment and the proactive

 © 2019 Royal Meteorological Society

adaptation of policy, practices and engineering design. Unlike logical prediction, used to test the truth of theories or the temporal prediction of near-term events such as weather, projections of future climate cannot be verified (Oreskes, 2000). Therefore applying climate change scenarios to climate risk assessment and adaptation planning requires both an ensemble of plausible model projections and measures of uncertainty, or as Oreskes (2000) suggested, "If the value of predictions is primarily political or social rather than epistemic, then we may need to be excruciatingly explicit about the uncertainties in the theory or model that produced them … ." The planners, engineers and policy makers responsible for adaptation planning often ask the obvious questions, "how likely are these projections?" and "when can we expect to notice climate change?." In this paper we attempt to address the latter query in particular by examining the uncertainty in climate projections, as well as the time of emergence (ToE) of climate change signals.

Analyses of model biases relative to historical observations and reanalysis data are relatively common, (see, e.g., Chapter 9 of the IPCC Fifth Assessment Report [IPCC AR5; Flato et al., 2013] and a recent paper on the capacity of regional climate models to simulate the climate of western Canada [Barrow and Sauchyn, 2017]). Less common is research which partitions the variance among model projections between signal, the simulated response to greenhouse gas forcing, and noise, the natural internal variability. Here, we examine the role of natural internal variability in (a) the time of emergence of noticeable climate change, and (b) the partitioning of model variance over time. The three main sources of uncertainty contained in projections of future climate from global and regional climate models (GCMs and RCMs) can be separated as follows (Hawkins and Sutton, 2009, 2011):

1. *Model uncertainty*: each model projects different future climate changes in response to the same radiative forcing. This results from incomplete knowledge constraining the climate model representation of physical and dynamical processes.
2. *Scenario uncertainty*: different assumptions about future emissions of greenhouse gases (GHGs), and thus future radiative forcing, result in uncertainty in the projection of future climate. This arises from a lack of knowledge of future GHG emission trajectories, involving unpredictable feedbacks between climatic and socio-economic factors.
3. *Natural internal variability*: these are the largely chaotic and unpredictable natural fluctuations in climate which arise in the absence of any radiative forcing and which are superimposed on the long-term trends in each projection of future climate; these fluctuations may mask, particularly in the near-term or enhance the signal of anthropogenic climate change. It is evident when several runs of a single climate model, with very similar external forcing and initial conditions, yield different results.

The IPCC AR5 (IPCC, 2013) included a discussion of these sources of uncertainty in climate model projections, representing them graphically as a "plume" and as a plot of the fractions of the total variance by lead time, climate variable and global versus regional scale (see Figure 11.8 in Kirtman et al., 2013). The plume depicts internal variability as constant through time, while the scenario and model uncertainties are shown as increasing. In the time series plots spanning the 21st century, global projections of climate change are dominated by model and scenario uncertainty, although internal variability is a significant source of uncertainty in the near term. This IPCC AR5 discussion of uncertainty is based primarily on the work of Hawkins and Sutton (2009, 2011) who emphasized that relative uncertainty can be very different at regional spatial scales. In their analysis of European winter climate, internal variability is relatively more important and for precipitation, scenario uncertainty is almost irrelevant.

The objective of this paper is to quantify the uncertainty in global climate model projections for Canada's western interior, documenting the relative amounts of model, scenario and internal variability uncertainty and the timing of the emergence of climate change signals. Our focus is on surface air temperature, precipitation and the climate moisture index (CMI; Hogg, 1994, 1997) in the three Prairie Provinces of Manitoba, Saskatchewan and Alberta. The hydroclimates of the northern Great Plains are among the most variable on Earth, with large temperature seasonality and inter-annual variability, given a mid-latitude continental location and strong teleconnections with Pacific and Arctic sea-surface temperature oscillations. Whereas climate projections at all scales are subject to the same sources of uncertainty, their relative magnitudes and natural internal variability in particular, will differ according to the nature of the regional climate regime and its sensitivity to anthropogenic interference in the global energy balance. Here, our focus is on the provision of meaningful information for local adaptation planning regarding the timing of noticeable climate change and the role of natural variability.

This work is related to studies of climate change and impacts in the South Saskatchewan River Basin (SSRB; Sauchyn et al., 2016) which included interactions (via interviews and presentations) with stakeholders, such as ranchers and farmers whose livelihoods depend on water availability in the SSRB watershed, as well as more rigorous scientific approaches, including hydrological modelling. This and other studies (e.g., Fennell et al., 2016; Jacques et al., 2010;

Pittman et al., 2011) have identified uncertainty in future climate as being one of the dominant stressors for farming/ranching communities and, thus, any further information we can provide on future uncertainty is of value to these communities.

2 | METHODOLOGY

2.1 | GCM output

GCM results from the most recent coupled model intercomparison project phase 5 (CMIP5) (Taylor et al., 2012; Sheffield et al., 2013; Maloney et al., 2014) provided the climate change projections used in this research. Since teleconnections such as the El Niño–Southern Oscillation (ENSO) and the Pacific Decadal Oscillation (PDO) impact the climatology and hydrology of western North America, including the Canadian prairies (Mantua et al., 1997; Higgins et al., 2000; Bonsal et al., 2001; Mantua and Hare, 2002; McCabe and Dettinger, 2002; Stewart et al., 2005; St. Jacques et al., 2010; Whitfield et al., 2010; Wise, 2010; Lapp et al., 2012; Meehl et al., 2013), a subset of 10 GCMs which better simulated ENSO and PDO conditions was selected for use in this study. These GCMs were identified by Sheffield et al. (2013) as being higher performance models in the simulation of near-surface air temperature and precipitation patterns over North America during El Niño and La Niña episodes. Since extratropical ENSO teleconnection dynamics are tied to upper-tropospheric processes and are strongest during the boreal winter, evaluation of the CMIP5 models was based on how well they reproduced the winter composite 300 hPa geopotential height patterns in the National Centers for Environmental Prediction/ National Center for Atmospheric Research (NCEP/NCAR) reanalysis. Sheffield et al. (2013) also showed that the CMIP5 models were able to capture the PDO influence on North American surface air temperature but did not do so well in reproducing precipitation patterns (although some of this may have been due to the sparsity of observed data for comparison in high latitudes). The characteristics of these 10 higher performance GCMs are listed in Table 1. We recognize that there is considerable uncertainty in the influence of ENSO on North American climate (e.g., Deser et al., 2017; Deser et al., 2018), and that typical responses to ENSO events do not necessarily occur in every episode, and hence other methods for assessing GCM performance in simulating ENSO (and PDO) may identify different models.

Output from the historical simulations and climate change runs for representative concentration pathways (RCPs) 2.6, 4.5, 6.0 and 8.5 (Moss et al., 2010) were downloaded and processed, totalling 37 realizations of future climate. These RCP values represent the radiative forcing in the year 2100 relative to pre-industrial values (so +2.6, +4.5, +6.0 and +8.5 Wm^{-2}). Where possible a single realization for each RCP was included in the dataset so that each GCM was considered equally. There were two exceptions to this: CanESM2 had runs for only RCP2.6, RCP4.5 and RCP8.5, while HadGEM2-CC had runs for only RCP4.5 and RCP8.5. The CMI (Hogg, 1994, 1997), a relatively simple measure of precipitation excess (or deficit) compared with potential evapotranspiration (PET) was calculated and totalled for the months of May, June and July and henceforth called summer CMI. PET was determined using a simplified Penman-Monteith method with altitude and maximum, minimum and mean temperatures as inputs. For each realization, a regional average value was calculated for western Canada. Changes from the 1986–2005 mean were then calculated for seasonal surface air temperature and precipitation, and for summer CMI. Ensemble-mean changes for each RCP were also calculated.

We also considered output from a further 24 CMIP5 GCMs, totalling 69 experiments, which had complete datasets for the four climate variables (precipitation, mean, maximum and minimum temperature) we required, in order to determine how the results from our subset of 10 GCMs compared with this larger dataset. Details for these additional GCMs are contained in Table S1.

2.2 | Variance partitioning

Following the methodology of Hawkins and Sutton (2009), the uncertainty in the projections of the selected CMIP5 GCM dataset was attributed to the three sources for seasonal mean surface air temperature and precipitation and summer CMI. Initially a fourth order polynomial was fitted to the model output time series using ordinary least squares for the period 1950–2099. Hawkins and Sutton (2009) then weighted the models used in their study by their ability to simulate the observed global mean warming, thus downplaying those models which warmed too much or too little. In our case, no weighting was applied since we had already pre-selected a subset of 10 GCMs considered to be better able to simulate the climate of western Canada, based on the results in Sheffield et al. (2013), as described earlier. The contributions of each of the three sources of uncertainty to the total variance of the projections were then calculated as follows:

- *Model uncertainty*: for each scenario this was estimated from the variance in the different model prediction fits. The multi-scenario mean of this variance was then taken as an estimate of the model uncertainty component.

TABLE 1 Details of the 10 higher performance CMIP5 models selected for study

GCM	Modelling centre	Horizontal resolution (°lon × °lat)	Available RCPs
BCC-CSM1-1	Beijing Climate Centre, Meteorological Administration, China	2.8 × 2.8	2.6, 4.5, 6.0, 8.5
CanESM2	Canadian Centre for Climate Modelling and Analysis	2.8 × 2.8	2.6, 4.5, 8.5
CCSM4	National Center for Atmospheric Research, USA	1.25 × 0.94	2.6, 4.5, 6.0, 8.5
GFDL CM3	NOAA/Geophysical Fluid Dynamics Laboratory, USA	2.5 × 2.0	2.6, 4.5, 6.0, 8.5
GISS-E2-R	NASA Goddard Institute for Space Studies, USA	2.5 × 2.0	2.6, 4.5, 6.0, 8.5
HadGEM2-CC	Met. Office Hadley Centre, UK	1.875 × 1.25	4.5, 8.5
IPSL-CM5A-LR	L'institut Pierre Simon Laplace, France	3.75 × 1.8	2.6, 4.5, 6.0, 8.5
IPSL-CM5A-MR	L'institut Pierre Simon Laplace, France	2.5 × 1.25	2.6, 4.5, 6.0, 8.5
MIROC5	Atmosphere and Ocean Research Institute (The University of Tokyo), National Institute for Environmental Studies, and Japan Agency for Marine-Earth Science and Technology, Japan	1.4 × 1.4	2.6, 4.5, 6.0, 8.5
NorESM1-M	Norwegian Climate Centre, Norway	2.5 × 1.9	2.6, 4.5, 6.0, 8.5

Note. For complete reference details for the CMIP5 GCMs, please see Table 9.A.1 in Flato et al. (2013).

- *Scenario uncertainty*: the variance of the multi-model means for the four scenarios (RCPs 2.6, 4.5, 6.0 and 8.5).
- *Natural internal variability*: the variance of the residuals after the fitting of the fourth order polynomial to each individual projection, calculated across all scenarios and time. The multi-model mean of these variances was taken to be the internal variability component and is constant in time.

2.3 | Time of emergence of climate signals

The ToE is a measure of when the climate change signal (S) emerges from the background noise (N) of natural climate variability. It can be calculated in a number of different ways since it depends on user-driven choices of climate variables, the spatial and temporal scales under consideration, the baseline time period relative to which changes are measured and the threshold at which emergence is defined (Kirtman et al., 2013). A number of different methods have been used to calculate the ToE (e.g., Christensen et al., 2007; Giorgi and Bi, 2009; Hawkins and Sutton, 2012; de Elía et al., 2013, 2014; Sui et al., 2014; Lehner et al., 2017; Li et al., 2017). In common with Sui et al. (2014), the inter-annual *SD* of the seasonal means provided our estimate of the climate noise. This was calculated using the pre-industrial control simulation from each of the GCMs in our selected subset; these control simulations varied in length from 251 to 1000 years, with most simulations being longer than 500 years. For each GCM, the time series of the signal from 1986 to 2099 was indicated by the change in 20-year running means relative to the baseline period of 1986–2005. Using 20-year running means filters out the inter-annual variability while retaining the multi-decadal variability of the signal (Giorgi and Bi, 2009). In contrast to Sui et al. (2014), who calculated a median signal and median noise from their GCM suite to obtain a median S/N ratio, we calculated the S/N ratio for each GCM before calculating the median ratio value. Latitudinally-weighted area averages of the grid-box S/N ratio values provided us with our regional average value for western Canada. In order to display the spatial distribution of median ToE, the grid box S/N values for each GCM were interpolated onto a common 2.5° latitude/longitude grid (the same resolution as that used in van Oldenborgh et al., 2013) using MATLAB's bilinear interpolation routine before the median S/N ratio and associated ToE were calculated.

Although the climate change signal first emerges from the background noise when S/N > 1, this does not necessarily mean that the signal is discernible. Using S/N > 2 is a more robust approach since the Student's *t* test indicates that a S/N value greater than 1.96 is required to reject the null hypothesis (S = N) at the 95% confidence level (de Elía et al., 2014) when sample sizes are sufficiently large (i.e., greater than 100). Although our sample size is small (with a critical t-value of 2.09 for a significant difference of means at the 95% confidence level), implying that our results are not necessarily robust, for simplicity we use S/N > 1 to indicate that climate signal has emerged from the noise of background variability, and S/N > 2 to identify a "significant" signal.

We also examined the pre-industrial control simulations to determine how S/N ratios in these simulations compared with those using the future climate projections. In this case, the long-term mean for each control simulation was used to represent baseline conditions and then the time series of the

signal for the length of the control simulation was indicated by the change in 20-year running means relative to this baseline. As above, the inter-annual *SD* of the seasonal means provided the noise estimate.

3 | RESULTS

3.1 | Changes in mean surface air temperature, precipitation and summer CMI

Figures 1–3 illustrate the changes (with respect to the 1986–2005 average) in mean surface air temperature, precipitation and summer CMI, respectively, for the period 1850–2100 for western Canada as a whole. Each of the 10 selected GCMs and an ensemble-mean value are illustrated for each of the four RCPs. On the right-hand side of each figure the range of results for each RCP is shown for the 24 additional GCMs. It is immediately apparent from these figures that the differences between the four RCPs are most distinct for surface air temperature (Figure 1) compared to precipitation (Figure 2) and summer CMI (Figure 3). For mean surface air temperature (Figure 1), variability is largest in winter and smallest in summer during both the historical and future simulations for both sets of GCM data. While ensemble-mean values for all RCPs indicate increases in future mean surface air temperature, and that these projected increases are largest in winter, projected changes in summer also are almost all positive, that is, consistently greater than the 1986–2005 mean value, in both the ensemble-mean values and the individual realizations. For the 24 additional GCMs, however, the lower bound of the future range is negative for all RCPs, indicating that values lower than the 1986–2005 mean occur in some realizations.

For precipitation (Figure 2), all seasons exhibit similar levels of variability and differences between the RCPs are not distinct. On the whole, the ensemble-mean projections show increased precipitation in winter, spring and fall, with RCP8.5 exhibiting the largest increase. In summer, ensemble-mean values indicate little change or, for RCP8.5, slight decreases in future precipitation when compared with the 1986–2005 mean. However, variability is large and individual realizations suggest decreases in precipitation which exceed 40% in some years. The 24 additional GCMs give similar results.

For summer CMI (Figure 3), ensemble-mean values for all RCPs indicate that future values for this index are significantly decreased, that is, they are lower than the 1986–2005 mean. The severity of this drying is largest for RCP8.5. Variability in projected values of summer CMI is large and while the trend is for drier conditions in the future, there are still years when index values are greater than the 1986–2005 mean. The data range for the 24 additional GCMs shows similar results.

3.2 | Variance partitioning

Figures 4–6 illustrate the contribution of each of the three uncertainty components to the total variance of decadal-mean surface air temperature, precipitation and summer CMI projections, respectively, for our subset of 10 GCMs. For all three variables, the internal variability uncertainty component (orange) is largest at the beginning of this

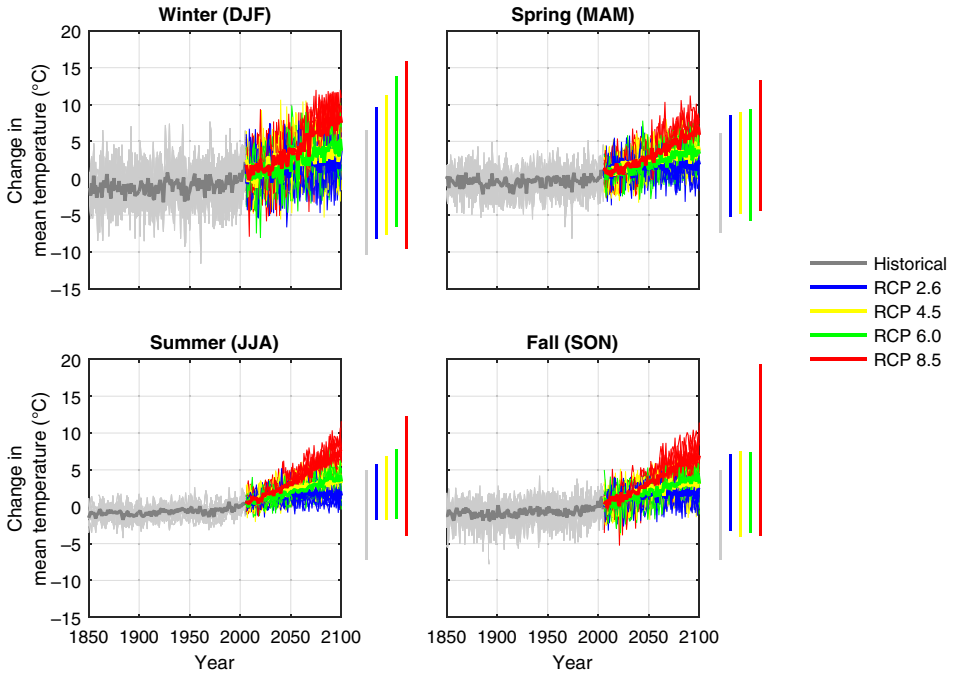

FIGURE 1 Change in mean surface air temperature (°C) for western Canada, 1850–2100, with respect to the 1986–2005 mean. Individual GCMs are indicated by fine coloured lines and ensemble-means by bold coloured lines. Vertical bars on the right-hand side of the figures indicate the range of results from 2006–2100 for the larger GCM dataset for comparison [Colour figure can be viewed at wileyonlinelibrary.com]

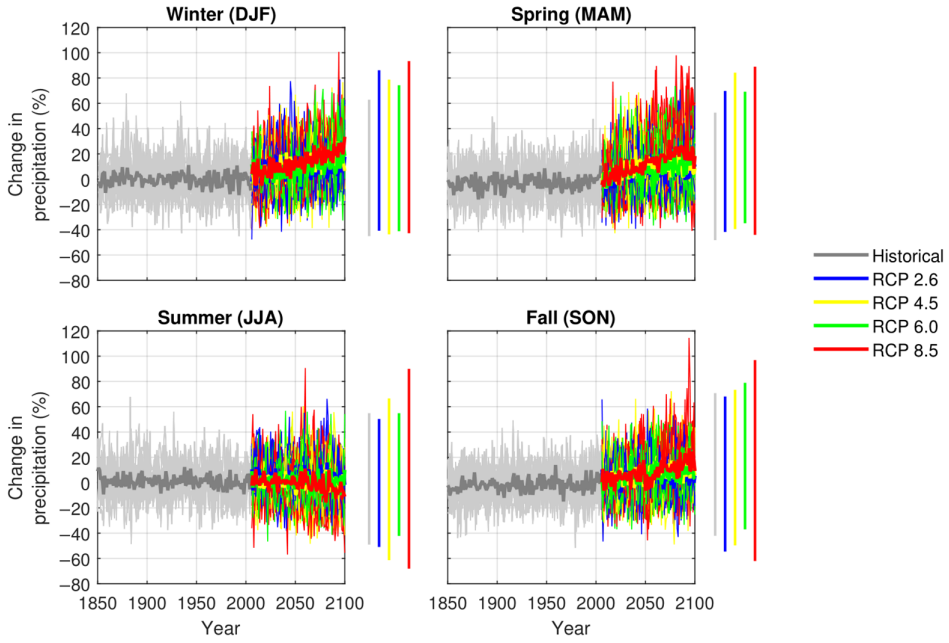

FIGURE 2 Change in precipitation (%) for western Canada, 1850–2100, with respect to the 1986–2005 mean. Individual GCMs are indicated by fine coloured lines and ensemble-means by bold coloured lines. Vertical bars on the right-hand side of the figures indicate the range of results from 2006–2100 for the larger GCM dataset for comparison [Colour figure can be viewed at wileyonlinelibrary.com]

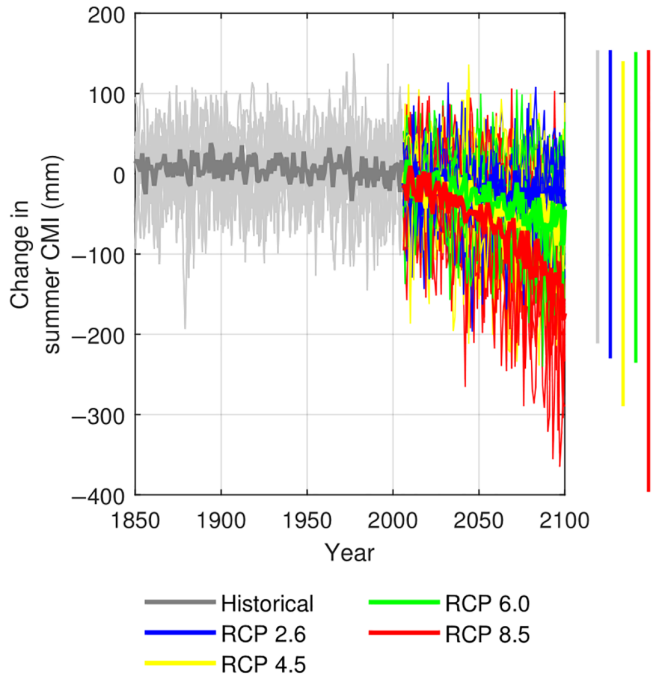

FIGURE 3 Change in summer CMI (mm) for western Canada, 1850–2100, with respect to the 1986–2005 mean. Individual GCMs are indicated by fine coloured lines and ensemble-means by bold coloured lines. Vertical bars on the right-hand side of the figures indicate the range of results from 2006–2100 for the larger GCM dataset for comparison [Colour figure can be viewed at wileyonlinelibrary.com]

century and decreases towards 2100. For mean surface air temperature (Figure 4), internal variability is largest in winter and spring, representing about 95% of the total variance initially and still approximately 40% of the total at the end of this century. In summer, this component represents only 10% of the total variance in temperature uncertainty at the end of this century. The model uncertainty component (blue) is largest in summer, but still represents only about 25% of total variance at mid-century; in other seasons it typically contributes between 5% and 15% of the total variance. The scenario uncertainty component (green) increases over time in all seasons and in summer represents about 70% of the total variance by the end of the century.

For precipitation (Figure 5), the internal variability and model uncertainty components are the major contributors to the total variance in the projections, with the scenario uncertainty component generally representing only about 5%–10% of the total by the end of the century. Model uncertainty is largest in spring and summer (approximately 45% and 25%, respectively, of the total variance in projections by 2100). Internal variability is very much the dominant source of uncertainty, accounting for more than 80% of the variance in the projections of fall and winter precipitation for the next several decades.

For summer CMI (Figure 6), internal variability accounts for about 95% of the total variance in projections at the beginning of the century; this decreases to about 30% by 2100. Scenario uncertainty does not contribute to the total variance in the projections until about 2025 and represents about 40% of total variance by 2100. The model uncertainty component increases from 5 to about 30% by the end of the century. Examination of Figures 4–6 indicates that these variance fractions for summer CMI are a hybrid of the results for summer temperature and precipitation, as would be expected given their role in the calculation of this variable. Internal variability and emission scenarios uncertainty play larger roles in future projection uncertainty for summer CMI compared to summer temperature and summer precipitation, respectively.

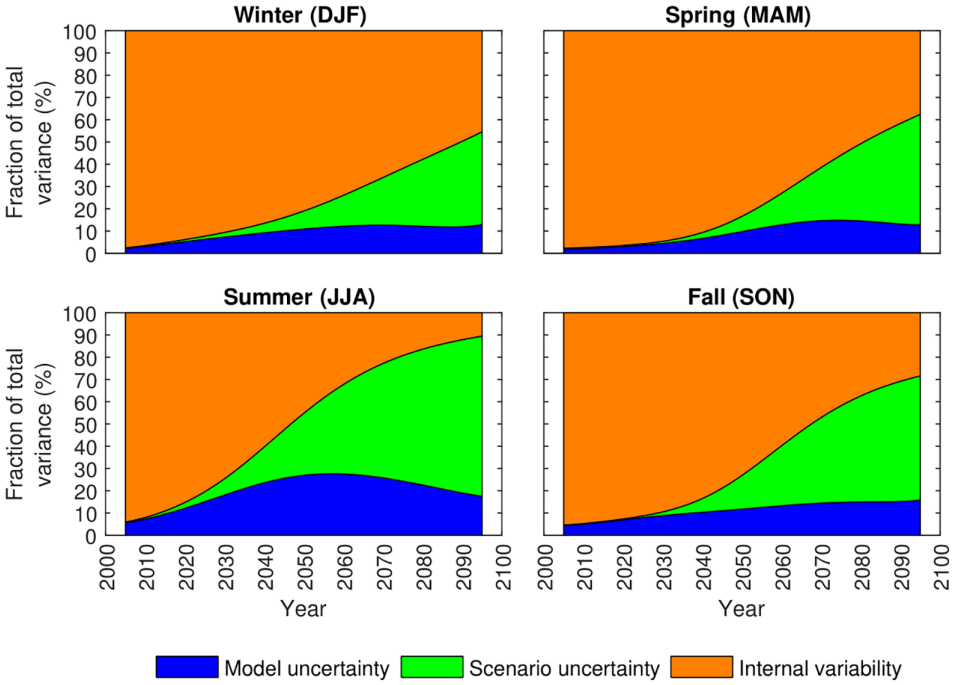

FIGURE 4 Fraction of total variance in decadal mean surface air temperature projections explained by internal variability, model uncertainty and scenario uncertainty for western Canada [Colour figure can be viewed at wileyonlinelibrary.com]

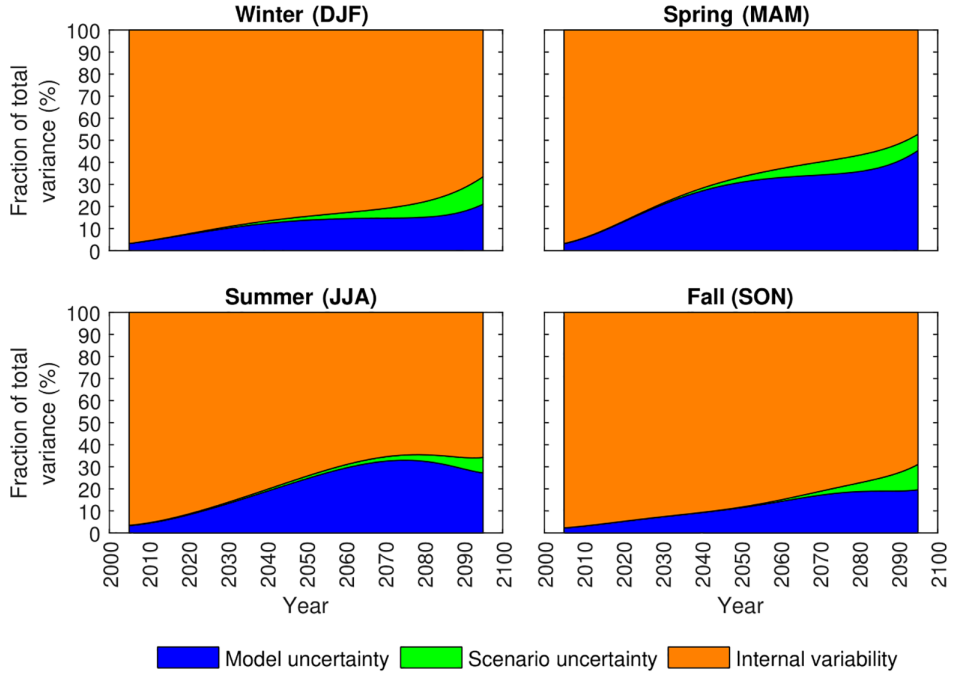

FIGURE 5 Fraction of total variance in decadal mean precipitation projections explained by internal variability, model uncertainty and scenario uncertainty for western Canada [Colour figure can be viewed at wileyonlinelibrary.com]

Examination of similar plots for our larger group of GCMs indicates very similar results (see Figures S1–S3 in the Supplementary Material). Given these results, we continue our analysis by considering only the subset of 10 GCMs.

3.3 | Time of emergence

S/N ratios calculated from the pre-industrial control simulations for mean temperature, precipitation and summer CMI showed very similar results (see Figures S4, S5 and S6 in the Supplementary Material). In all cases, S/N ratios did not exceed ±1 and very rarely exceeded ±0.5. Examination of S/N ratios at the grid scale yielded similar results (not shown).

Although ToE and S/N ratios were calculated for all RCPs, for conciseness results are shown only for RCP8.5 for western Canada as a whole (Figures 7–9). The increase in global carbon emissions over the last two decades has been consistent with higher scenarios, such as RCP8.5 (Hayhoe et al., 2017). Note that years

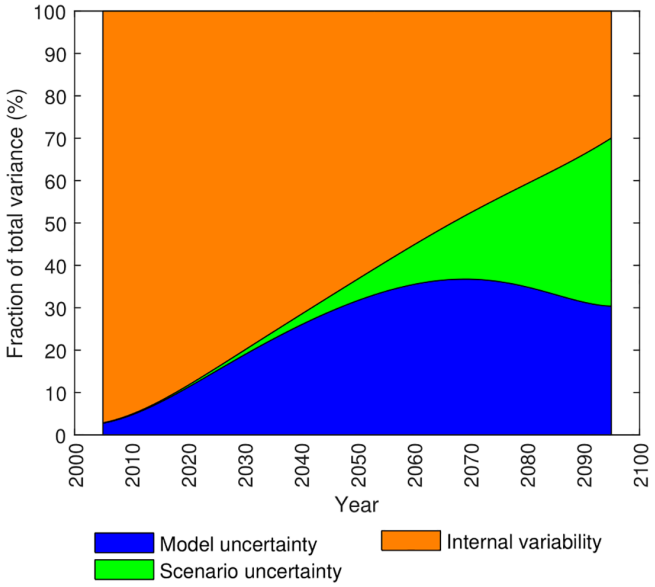

FIGURE 6 Fraction of total variance in decadal mean summer CMI projections explained by internal variability, model uncertainty and scenario uncertainty for western Canada [Colour figure can be viewed at wileyonlinelibrary.com]

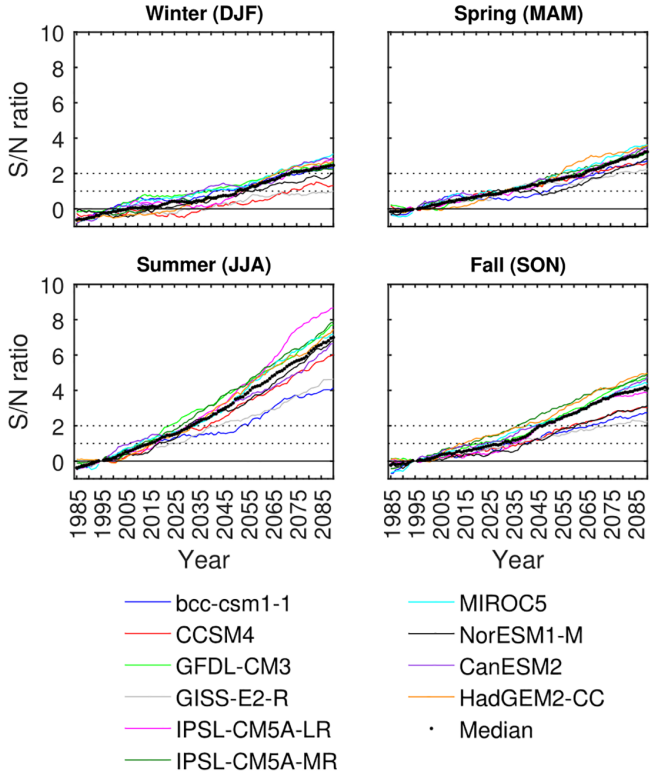

FIGURE 7 Signal-to-noise ratio for western Canada mean surface air temperature for RCP 8.5. Each coloured line denotes a different GCM. Black dots indicate median values. Dashed lines indicate threshold values [Colour figure can be viewed at wileyonlinelibrary.com]

correspond to the mid-point of the 20-year period under consideration (so, e.g., plotting starts at 1986 which represents the mid-point of the 1976–1995 20-year period). For the first eleven 20-year periods (up to 1985–2005) model output is used from the historical runs; historical and future runs are combined up to the 20-year period 2005–2024 and thereafter model output is from the future runs only.

For RCP8.5, the ToE of the mean surface air temperature change signal (Figure 7) varies by GCM, with the largest spread among the GCMs occurring in summer. In this season, S/N > 1 for almost all GCMs in the 20-year period centred on 2015. The earliest occurrence of S/N > 2 is about 2020, and by about 2055 S/N is always greater than two for all GCMs. The median S/N ratio indicates that the climate change signal emerges from the background noise (S/N > 1) around 2015 but does not become significant (S/N > 2) until about 2035. For winter, the earliest occurrence of S/N > 1 is about 2035, and all GCMs exhibit values greater than this by about 2080. The median ToE for S/N > 1 is around 2055, and becomes significant about 20 years later, in 2075. Not all GCM results are significant by the end of the century, although all indicate that S has emerged from N by this time. With the exception of the winter season, all GCMs indicate significant results by about 2075. ToE values generally indicate that the 2 S/N thresholds considered here are exceeded earlier for RCP8.5 and later for RCP2.6, as would generally be expected. Both S/N thresholds are exceeded earlier in fall (median value for significant change is 2050) than in spring (significant change occurs by about 2065) for RCP8.5, and the other RCPs also exhibit the same behaviour for these seasons.

For precipitation (and summer CMI), we consider both positive and negative threshold values, that is, ±1 and ±2, since future projections indicate both increases and decreases in these variables. Figure 8 illustrates that for precipitation there is more variability in S/N values in spring and summer than in fall and winter and that values for individual GCMs do not necessarily consistently exceed S/N threshold values, which is the case for mean surface air temperature. All GCMs project increases (positive S/N values) in future winter precipitation, compared to the 1986–2005 baseline. While the median signal emerges from the noise around 2075 in winter and around 2080 in spring, significant results (i.e., S/N > 2) are not obtained before the end of the century in any season. Only a single GCM, BCC-CSM1-1, indicates a significant increase in precipitation from about 2075 onwards in winter. For summer, S/N ratios are both positive and negative, with median values hovering around zero before becoming slightly negative towards the end of the century. For RCP2.6, median S/N values indicate that the signal does not emerge from the noise in any of the seasons, or for summer and fall for RCPs 4.5 and 6.0 (not shown).

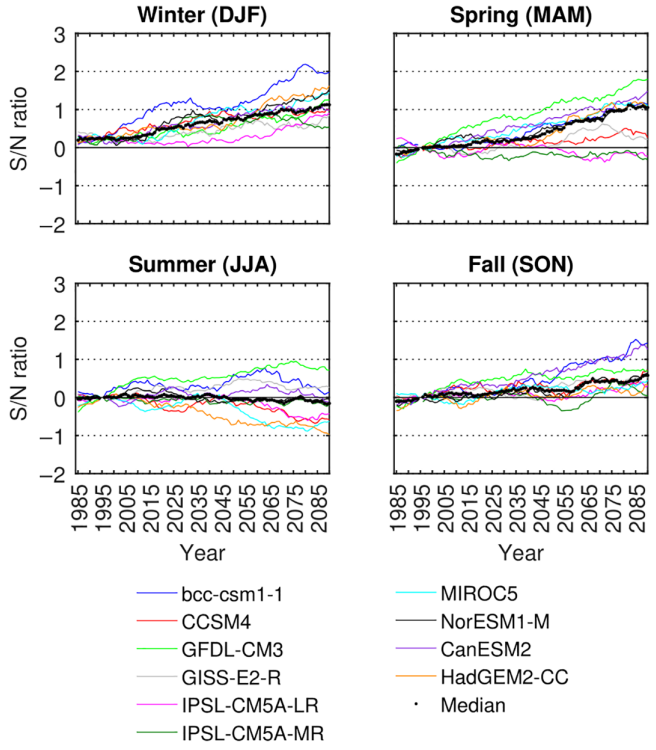

FIGURE 8 Signal-to-noise ratio for western Canada precipitation for RCP8.5. Each coloured line denotes a different GCM. Black dots indicate median values. Dashed lines indicate threshold values [Colour figure can be viewed at wileyonlinelibrary.com]

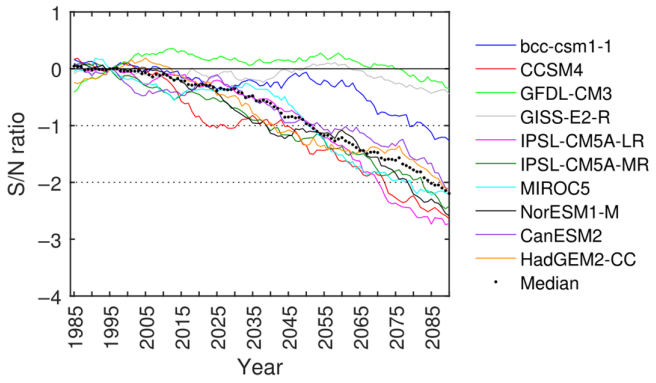

FIGURE 9 Signal-to-noise ratio for western Canada summer CMI for RCP 8.5. Each coloured line denotes a different GCM. Black dots indicate median values. Dashed lines indicate threshold values [Colour figure can be viewed at wileyonlinelibrary.com]

Figure 9 shows the S/N ratio time series for summer CMI. The majority of the GCMs considered here indicate drier future conditions (i.e., negative S/N ratios) than those of the baseline period. The median signal first emerges from the noise about 2050 and becomes significant towards the end of the century, around 2085. With the exception of GFDL-CM3, GISS-E2-R and BCC-CSM1-1, all GCMs indicate significant S/N values by the end of the century, with

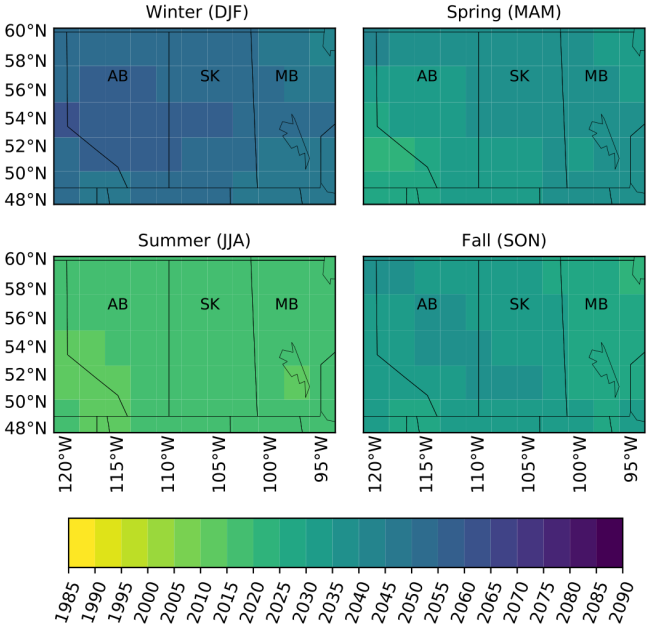

FIGURE 10 Median ToE for mean temperature for S/N = 1 for RCP8.5. Dates indicate the centre value of the 20-year period. White areas indicate where the signal does not emerge in the study time period. AB, Alberta; MB, Manitoba; SK, Saskatchewan [Colour figure can be viewed at wileyonlinelibrary.com]

IPSL-CM5A-LR exhibiting the earliest significant result, between 2070 and 2075. The PET component of the summer CMI, which is temperature driven, exceeds the precipitation component and this results in these signal-to-noise ratios which indicate emergence of the climate change signal about 2050 and significant change by the end of the century. Neither threshold is exceeded for RCP2.6, and S/N = 2 is not exceeded for RCP4.5 (not shown).

The median ToE of climate change signals for RCP8.5 was also examined on a grid-box by grid-box basis for western Canada, as described earlier. The median ToE was defined as the time at which the median S/N ratio crossed the two thresholds considered (S/N = 1 and S/N = 2) and remained *consistently above* those thresholds during the study period. Results are shown in Figures 10–14.

For mean surface air temperature, the signal emerges from background noise (S/N > 1) earliest in summer, with median ToEs between 2010 and 2020 (Figure 10) and becomes significant (S/N > 2) in this season between 2020 and 2035 (Figure 11). Latest emergence for S/N > 1 and S/N > 2 occurs in the west central prairies in winter, around 2055 and after 2070, respectively. For precipitation (Figure 12), the S/N = 1 threshold is not exceeded at all in summer or in the majority of grid boxes in spring and fall, that is, in general the signal does not emerge from the noise in these seasons during this century. In the handful of grid boxes where the signal does emerge in spring and fall, it is generally towards the end of the study period, certainly after

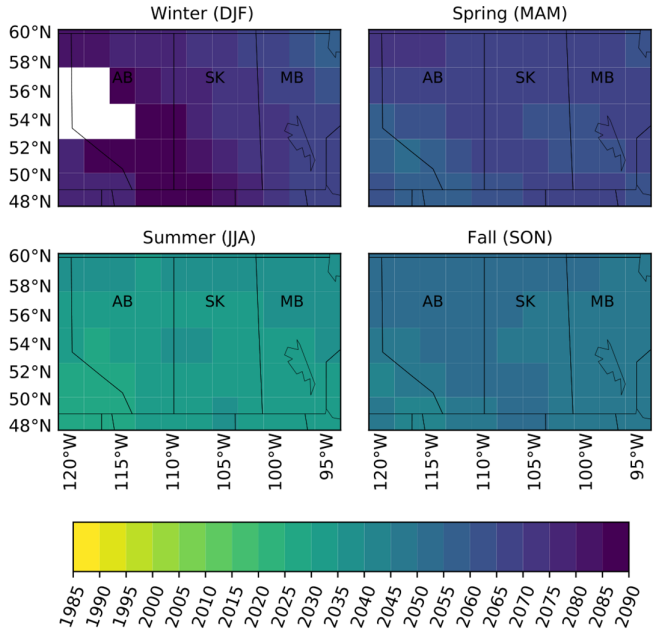

FIGURE 11 Median ToE for mean temperature for S/N = 2 for RCP8.5. Dates indicate the centre value of the 20-year period. White areas indicate where the signal does not emerge in the study time period. AB, Alberta; MB, Manitoba; SK, Saskatchewan [Colour figure can be viewed at wileyonlinelibrary.com]

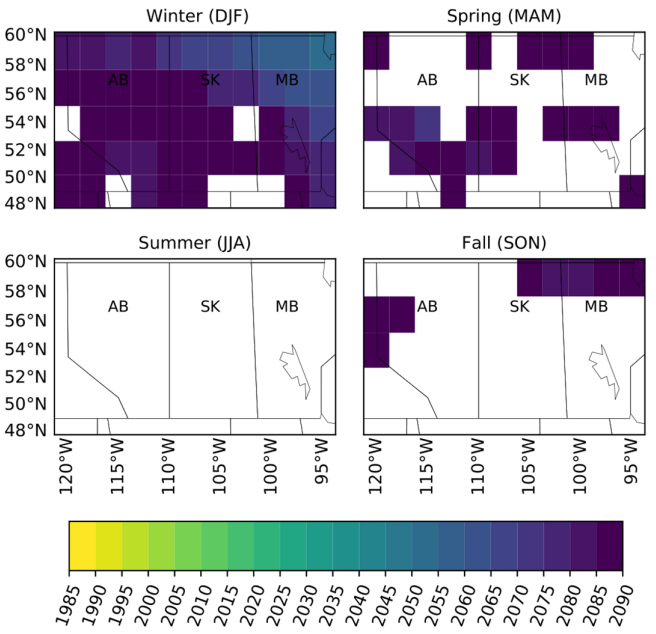

FIGURE 12 Median ToE for precipitation for S/N = 1 for RCP8.5. Dates indicate the centre value of the 20-year period. White areas indicate where the signal does not emerge in the study time period. AB, Alberta; MB, Manitoba; SK, Saskatchewan [Colour figure can be viewed at wileyonlinelibrary.com]

2075. In winter, the S/N > 1 threshold is exceeded earliest in the northeast of the region, with median ToE around 2050, and later elsewhere (2080s onwards). In some grid

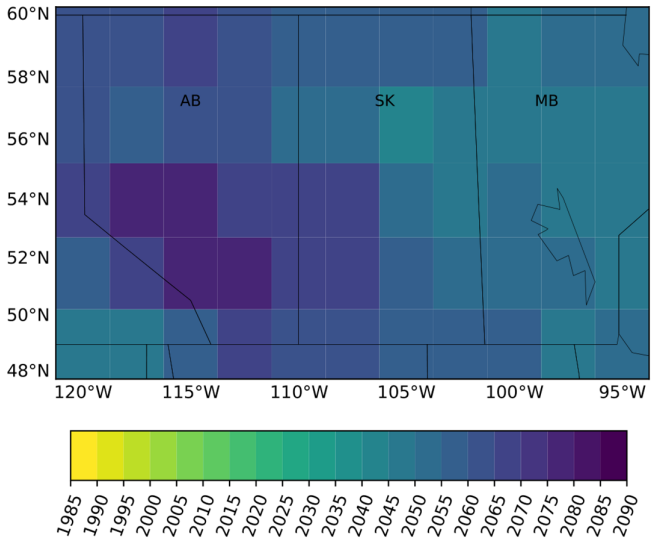

FIGURE 13 Median ToE for summer CMI for S/N = 1 for RCP8.5. Dates indicate the centre value of the 20-year period. White areas indicate where the signal does not emerge in the study time period. AB, Alberta; MB, Manitoba; SK, Saskatchewan [Colour figure can be viewed at wileyonlinelibrary.com]

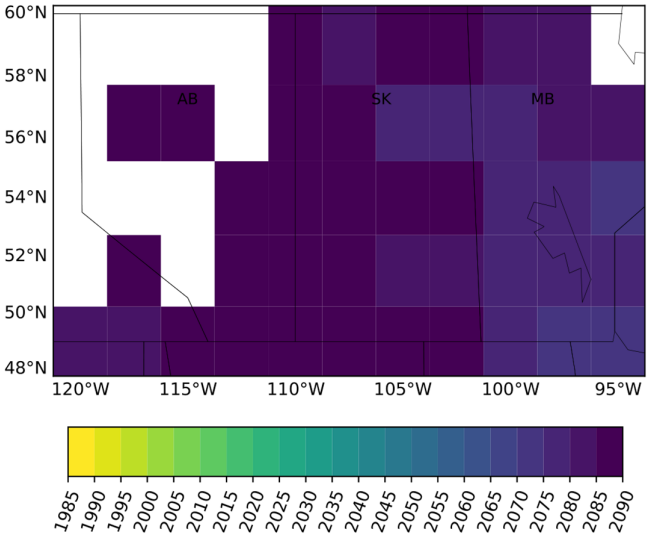

FIGURE 14 Median ToE for summer CMI for S/N = 2 for RCP8.5. Dates indicate the centre value of the 20-year period. White areas indicate where the signal does not emerge in the study time period. AB, Alberta; MB, Manitoba; SK, Saskatchewan [Colour figure can be viewed at wileyonlinelibrary.com]

boxes in central and southern areas, this threshold is not exceeded in this season this century. With the exception of the winter season, where three grid boxes in the north-easternmost corner of the study region exhibit median times of emergence in the 2080s and later, significant signals are not obtained in any season (not shown). For summer CMI (Figure 13), median ToE for S/N > 1 is between 2035 and 2075, with later emergence generally being in the west of

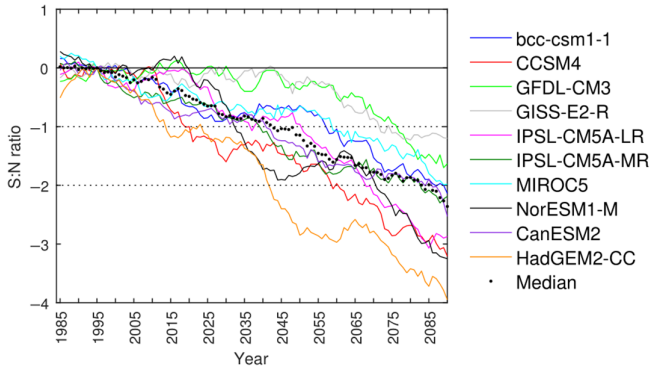

FIGURE 15 Signal-to-noise ratio for summer CMI for each GCM for RCP8.5 for a single grid box in the south-west corner of the Prairie Provinces [Colour figure can be viewed at wileyonlinelibrary.com]

the region. The median ToE of significant signals (S/N > 2; Figure 14) is between 2065 and the end of the century, with earliest emergence occurring in the eastern half of the region, between 2065 and 2070. Some grid boxes in Alberta do not show significant signals this century. Figure 15 illustrates the S/N ratio for summer CMI for a single grid box in the southwest corner of the region for each GCM. This plot indicates that, while the general trend is for drier conditions, that is, decreases in summer CMI, times of signal emergence (S/N > 1) and significant (S/N > 2) change can vary considerably. By the end of the century, the signal has emerged from the background noise for all GCMs (as early as 2015 for HadGEM2-CC and as late as 2075 for GFDL-CM3) but is not significant by this time for GFDL-CM3, GISS-E2-R and MIROC5. HadGEM2-CC, however, exhibits the earliest significant signal, in the early 2040s.

4 | DISCUSSION AND CONCLUSIONS

Many climate change studies provide projected changes in weather variables, primarily temperature and precipitation, for different greenhouse gas emissions scenarios, to determine impacts on sectors such as water resources and agriculture. However, for decision-makers and adaptation planning, the range and probability of these projected changes is of more importance than the absolute magnitude of the projected changes (Hawkins and Sutton, 2012). For the Prairie Provinces of western Canada, this paper has examined the relative significance of uncertainty in future climate projections from a subset of the CMIP5 GCMs in two ways:

1. By determining the contribution of the three main sources of uncertainty (model, scenario, natural variability) to the total variance of these future projections, and
2. By determining the timing of the emergence of the climate signal, using two different thresholds, from the background of natural climate variability.

In regions where natural climate variability is large, climate is less predictable. By partitioning the three main sources of uncertainty in the climate projections considered here, we have shown that natural climate variability plays an important role in future projection uncertainty until at least mid-century for all variables. The exception to this is summer mean surface air temperature, where both model and scenario uncertainty grow in importance over time, so that by the end of the century natural variability represents only 10% of the total variance in projections in this season, compared to between 30% and 40% in the other seasons. For precipitation, however, natural variability continues to account for between 40% and 60% of the total variance by the end of this century, with model uncertainty being the next largest contributor. Scenario uncertainty represents only 5%–10% of the variance in precipitation projections by the end of the century; this supports the results illustrated in Figure 2, which shows that it is more difficult to distinguish between the different radiative forcing scenario projections for this variable than for mean temperature or summer CMI. For summer CMI, calculated from both temperature and precipitation variables, the natural variability component of uncertainty gradually decreases from 95% at the beginning of the study period to about 30% at the end of the century, with model and scenario uncertainty contributing almost equally at the end of the century. While model and scenario uncertainty may be reduced as climate models improve and emissions projections become more accurate, the uncertainty attributable to the natural variability of future climate cannot be reduced (Deser et al., 2012).

In order to examine the significance of the projected future changes, we looked at the time when the climate change signal exceeds natural climate variability, that is, the time of emergence (ToE). This is a key question for adaptation policy and planning since, in general, natural and man-made systems are inherently adapted to the local levels of natural variability. It is only when changes move outside of this range that major impacts will possibly occur (Hawkins and Sutton, 2012). Although the climate change signal emerges from background noise when S/N > 1, it may not be discernible at this threshold and so we used S/N > 2 to define a significant signal. When exactly significant climate change becomes visible will vary with location and season. Our results indicate that the median mean summer surface air temperature signal across the prairie region emerges from the background noise in the 20-year period centred on 2015 and becomes significant around 2030, compared with 2055 and 2075, respectively, for the winter season. This is in keeping with results from

Christensen et al. (2007), Mahlstein et al. (2011) and Hawkins and Sutton (2012), which showed that the earliest ToE for significant warming in most regions is in the summer season. Lehner et al. (2017) examined ToE in summer surface air temperature observations and, after dynamical adjustment to account for the effect of atmospheric circulation changes on natural variability, calculated ToE as between 2000 and 2010 in our study region, although uncertainty in these results is greater than 10%. Using a large ensemble of simulations from the community earth system model (CESM) GCM, Lehner et al. (2017) showed that the forced warming signal emerges earlier in the observations than is suggested by the models. Examination of the pre-industrial S/N ratios here indicated that values rarely exceeded ±0.5, thus indicating that significant signals do not occur in an unforced climate.

For the GCMs considered here, times of emergence for precipitation are more variable and not always consistent, that is, the signal may emerge from the background noise, but does not necessarily remain so throughout the time period under consideration. Median S/N ratios indicate that the signal emerges from the background noise by about 2070 in winter and slightly later in spring, but significant S/N values (i.e., >2) do not occur in any season. Use of a wider smoothing window (e.g., 30 years rather than 20) for this variable might facilitate more robust ToE detection since this variable has a larger intrinsic variability than mean temperature (Curry, personal communication). In contrast to mean air surface temperature, the precipitation signal is not generally significant (S/N > 2) on a grid-box by grid-box basis in any season, although the signal does emerge from the background noise in winter over most of the region towards the end of the century. This is slightly later than results from Christensen et al. (2007) and Giorgi and Bi (2009) which indicated ToE as being in the middle of this century for mid-latitude areas in the northern hemisphere.

A key message from the results of this study is that resolving differences among climate models could reduce the uncertainty in projections, but it is still largely irreducible due to internal climatic variability. Deser et al. (2012, 2014) and Fischer et al. (2013) reached similar conclusions from experiments using large ensembles of projections from earth system models. Deser et al. (2012) suggested that the limits on climate prediction imposed by natural variability are most severe in the mid to high latitudes of North America and in boreal winter; that is, in the critical season for the natural storage of water for our targeted region. We have shown that natural variability uncertainty is the largest contributor to uncertainty in precipitation projections in our region, continuing to contribute between 45% and 65%, depending on season, at the end of the century.

Further evidence in our results of the influence of natural variability is fluctuations in the time of emergence of a climate change signal in projections of precipitation and summer CMI. S/N ratios vary considerably among GCMs. Median ToE for precipitation indicates that while the signal emerges from the background noise by the 2070s in winter and spring for the region as a whole, significant precipitation change is not seen this century in any season. For summer CMI, median ToE for significant change occurs about 2085, although not all GCM results suggest significant change by the end of the century, and for two GCMs, GFDL-CM3 and GISS-E2-R, the signal has not emerged from the noise by this time. Other analyses similar to ours, but for other continents (Hawkins and Sutton, 2009, 2011; Kirtman et al., 2013, Sui et al., 2014), point to the significance of natural variability, but not to the same extent as in our findings. This outcome was anticipated from global weather data showing that only east-central Asia (Siberia/Mongolia) has greater temperature seasonality (and comparable inter-annual variability) than the northern plains of North America. Paleoclimate (tree-ring) data from this region (e.g., Sauchyn et al., 2015; Sauchyn and Ilich, 2017) reveal a range of hydroclimate over the past millennium that exceeds observations, display significant modes of natural variability at annual and decadal scales, and include episodes of wet and dry climate of greater amplitude and duration than in the instrumental record.

The results of this study provide planners, policy makers and engineers in western Canada with regionally relevant measures of uncertainty. Whereas model uncertainty is important at all timescales, and emissions scenarios are relevant in the longer term, natural variability is critical over the next several decades, which correspond to the planning horizon of concern to most practitioners. These results emphasize that reduction in uncertainty in future projections is potentially limited in this region since the role of natural variability is large, especially for precipitation. This work informs the use of climate model projections in this region and the application of climate science to impacts assessment and adaptation planning. The climate of future decades, while increasingly human altered, will also reflect to a large extent the natural internal variability of the regional hydroclimate and stochastic atmospheric processes.

ACKNOWLEDGEMENTS

This work was funded by the Climate Research Branch of Environment and Climate Change Canada. We thank Dr. Marjorie Shepherd for her support.

We acknowledge the World Climate Research Programme's Working Group on Coupled Modelling, which is responsible for the CMIP, and we thank the climate modelling groups (listed in Tables 1 and S1 of this paper) for producing and making available their model output. For the CMIP the U.S. Department of Energy's Program for Climate Model Diagnosis and Intercomparison provides coordinating support and led development of software

infrastructure in partnership with the Global Organization for Earth System Science Portals.

We thank Yuliya Andreichuk for help with CMIP5 data download.

Finally, we thank Charles Curry and the other reviewers for their helpful and thoughtful comments which have improved this paper.

ORCID

Elaine M. Barrow https://orcid.org/0000-0003-3087-7172

REFERENCES

Barrow, E.M. and Sauchyn, D.J. (2017) An analysis of the performance of RCMs in simulating current climate over Western Canada. *International Journal of Climatology*, 37 (Suppl. 1), 640–658. https://doi.org/10.1002/joc.5028.

Bonsal, B.R., Shabbar, A. and Higuchi, K. (2001) Impact of low frequency variability modes on Canadian winter temperature. *International Journal of Climatology*, 21, 95–108.

Christensen, J.H., Hewitson, B., Busuioc, A., Chen, A., Gao, X., Held, I., Jones, R., Kolli, R.K., Kwon, W.-T., Laprise, R., Magana Rueda, V., Mearns, L., Menendez, C.G., Raisanen, J., Rinke, A., Sarr, A. and Whetton, P. (2007) Regional climate projections. In: Solomon, S., Qin, D., Manning, M., Chen, Z., Marquis, M., Averyt, K.B., Tignor, M. and Miller, H.L. (Eds.) *Climate Change 2007: The Physical Science Basis. Contribution of Working Group 1 to the Fourth Assessment Report of the Intergovernmental Panel on Climate Change*. Cambridge: Cambridge University Press, pp. 847–940.

Deser, C., Simpson, I.R., Phillips, A.S. and McKinnon, K.A. (2018) How well do we know ENSO's climate impacts over North America, and how do we evaluate models accordingly? *Journal of Climate*, 31, 4991–5014. https://doi.org/10.1175/JCLI-D-17-0783.1.

Deser, C., Simpson, I.R., McKinnon, K.A. and Phillips, A.S. (2017) The Northern Hemisphere extratropical atmospheric circulation response to ENSO: how well do we know it and how do we evaluate models accordingly. *Journal of Climate*, 30, 5059–5082. https://doi.org/10.1175/JCLI-D-16-0792.1.

Deser, C., Phillips, A.S., Alexander, M.A. and Smoliak, B.V. (2014) Projecting North American climate over the next 50 years: uncertainty due to internal variability. *Journal of Climate*, 27, 2271–2296. https://doi.org/10.1175/JCLI-D-13-00451.1.

Deser, C., Phillips, A., Bourdette, V. and Teng, H. (2012) Uncertainty in climate change projections: the role of internal variability. *Climate Dynamics*, 38, 527–546.

de Elía, R., Biner, S., Frignon, A. and Côté, H. (2014) Timescales associated with climate change and their relevance in adaptation strategies. *Climatic Change*, 126, 93–106. https://doi.org/10.1007/s10584-014-1209-x.

de Elía, R., Biner, S. and Frignon, A. (2013) Interannual variability and expected regional climate change over North America. *Climate Dynamics*, 41, 1245–1267. https://doi.org/10.1007/s00382-013-1717-9.

Fennell, K.M., Jarrett, C.E., Kettler, L.J., Dollman, J. and Turnbull, D. A. (2016) Watching the bank balance build up then blow away and the rain clouds do the same. A thematic analysis of South Australian farmers' sources of stress during drought. *Journal of Rural Studies*, 46, 102–110.

Fischer, E.M., Beyerle, U. and Knutti, R. (2013) Robust spatially aggregated projections of climate extremes. *Nature Climate Change*, 3, 1033–1038. https://doi.org/10.1038/NCLIMATE2051.

Flato, G., Marotzke, J., Abiodun, B., Braconnot, P., Chou, S.C., Collins, W., Cox, P., Driouech, F., Emori, S., Eyring, V., Forest, C., Gleckler, P., Guilyardi, E., Jakob, C., Kattsov, V., Reason, C. and Rummukainen, M. (2013) Evaluation of climate models. In: Stocker, T.F., Qin, D., Plattner, G.-K., Tignor, M., Allen, S.K., Boschung, J., Nauels, A., Xia, Y., Bex, V. and Midgley, P.M. (Eds.) *Climate Change 2013: The Physical Science Basis. Contribution of Working Group I to the Fifth Assessment Report of the Intergovernmental Panel on Climate Change*. Cambridge; New York, NY: Cambridge University Press, pp. 741–866.

Giorgi, F. and Bi, X. (2009) Time of emergence (TOE) of GHG-forced precipitation change hot-spots. *Geophysical Research Letters*, 36, L06709. https://doi.org/10.1029/2009GL037593.

Hawkins, E. and Sutton, R. (2009) The potential to narrow uncertainty in regional climate predictions. *Bulletin of the American Meteorological Society*, 90, 1095–1107.

Hawkins, E. and Sutton, R. (2011) The potential to narrow uncertainty in projections of regional precipitation change. *Climate Dynamics*, 37, 407–418.

Hawkins, E. and Sutton, R. (2012) Time of emergence of climate signals. *Geophysical Research Letters*, 39, L01702. doi: 10.29/2011GL050087.

Hayhoe, K., Edmonds, J., Kopp, R.E., LeGrande, A.N., Sanderson, B. M., Wehner, M.F. and Wuebbles, D.J. (2017) Climate models, scenarios and projections. In: Wuebbles, D.J., Fahey, D.W., Hibbard, K.A., Dokken, D.J., Stewart, B.C. and Maycock, T.K. (Eds.) *Climate Science Special Report: Fourth National Climate Assessment, Volume 1*. Washington, D.C.: US Global Change Research Program, pp. 133–160. https://doi.org/10.7930/J0WH2N54.

Higgins, R.W., Leetmaa, A., Xue, Y. and Barnston, A. (2000) Dominant factors influencing the seasonal predictability of U.S. precipitation and surface air temperature. *Journal of Climate*, 13, 3994–4017.

Hogg, E.H. (1997) Temporal scaling of moisture and the forest-grassland boundary in western Canada. *Agricultural and Forest Meteorology*, 84, 115–112.

Hogg, E.H. (1994) Climate and the southern limit of the western Canadian boreal forest. *Canadian Journal of Forest Research*, 24, 1835–1845.

IPCC. (2013) In: Stocker, T.F., Qin, D., Plattner, G.-K., Tignor, M., Allen, S.K., Boschung, J., Nauels, A., Xia, Y., Bex, V. and Midgley, P.M. (Eds.) *Climate Change 2013: The Physical Science Basis. Contribution of Working Group I to the Fifth Assessment Report of the Intergovernmental Panel on Climate Change*. Cambridge; New York, NY: Cambridge University Press, p. 1535.

Jacques, L.-S., De Vit, C. and Gagnon-Lebrun, F. (2010) *Status of Climate Change Adaptation in Canada's Agricultural Sector*. Ottawa: Government of Canada, p. 28.

Kirtman, B., Power, S.B., Adedoyin, J.A., Boer, G.J., Bojariu, R., Camilloni, I., Doblas-Reyes, F.J., Fiore, A.M., Kimoto, M., Meehl, G.A., Prather, M., Sarr, A., Schar, C., Sutton, R., van Oldenborgh, G.J., Vecchi, G. and Wang, H.J. (2013) Near-term climate change projections and predictability. In: Stocker, T.F., Qin, D., Plattner, G.-K., Tignor, M., Allen, S.K., Boschung, J., Nauels, A., Xia, Y., Bex, V. and Midgley, P.M. (Eds.) *Climate Change 2013: The Physical Science Basis. Contribution of*

Working Group 1 to the Fifth Assessment Report of the Intergovernmental Panel on Climate Change. Cambridge: Cambridge University Press, pp. 953–1028.

Lapp, S.L., St. Jacques, J.-M., Barrow, E.M. and Sauchyn, D.J. (2012) GCM projections for the Pacific decadal oscillation under greenhouse forcing for the early 21st century. *International Journal of Climatology*, 32, 1423–1442.

Lehner, F., Deser, C. and Terray, L. (2017) Towards a new estimate of 'time of emergence' of anthropogenic warming: insights from dynamical adjustment and a large initial-condition model ensemble. *Journal of Climate*, 30, 7739–7756. https://doi.org/10.1175/JCLI-D-16-0792.1.

Li, J., Thompson, D.W., Barnes, E.A. and Solomon, S. (2017) Quantifying the lead time required for a linear trend to emerge from natural climate variability. *Journal of Climate*, 30, 10179–10191. https://doi.org/10.1175/JCLI-D-16-0280.1.

Mahlstein, I., Knutti, R., Solomon, S. and Portmann, R.W. (2011) Early onset of significant local warming in low latitude countries. *Environmental Research Letters*, 6, 034009. https://doi.org/10.1088/1748-9326/6/3/034009.

Maloney, E.D., Camargo, S.J., Chang, E., Colle, B., Fu, R., Geil, K.L., Hu, Q., Jiang, X., Johnson, N., Karnauskas, K.B., Kinter, J., Kirtman, B., Kumar, S., Langenbrunner, B., Lombardo, K., Long, L. N., Mariotti, A., Meyerson, J.E., Mo, K.C., Neelin, J.D., Pan, Z., Seager, R., Serra, Y., Seth, A., Sheffield, J., Stroeve, J., Thibeault, J., Xie, S.-P., Wang, C., Wyman, B. and Zhao, M. (2014) North American climate in CMIP5 experiments: part III: assessment of 21st century projections. *Journal of Climate*, 27, 2230–2270.

Mantua, N.J. and Hare, S.R. (2002) The Pacific decadal oscillation. *Journal of Oceanography*, 58, 35–44.

Mantua, N.J., Hare, S.R., Zhang, Y., Wallace, J.M. and Francis, R.C. (1997) A Pacific interdecadal climate oscillation with impacts on salmon production. *Bulletin of the American Meteorological Society*, 78, 1069–1079.

McCabe, G.J. and Dettinger, M.J. (2002) Primary modes and predictability of year-to-year snowpack variations in the western United States from teleconnections with Pacific Ocean climate. *Journal of Hydrometeorology*, 3, 13–25.

Meehl, G.A., Hu, A., Arblaster, J., Fasullo, J. and Trenberth, K.E. (2013) Externally forced and internally generated decadal climate variability associated with the interdecadal Pacific oscillation. *Journal of Climate*, 26, 7298–7310.

Moss, R.H., Edmonds, J.A., Hibbard, K.A., Manning, M.R., Rose, S.K., van Vuuren, D.P., Carter, T.R., Emori, S., Kainuma, M., Kram, T., Meehl, G.A., Mitchell, J.F.B., Nakicenovic, N., Riahi, K., Smith, S.J., Stouffer, R.J., Thomson, A.M., Weyant, J.P. and Wilbanks, T.J. (2010) The next generation of scenarios for climate change research and assessment. *Nature*, 463, 747–756. https://doi.org/10.1038/nature08823.

van Oldenborgh, G., Collins, M., Arblaster, J., Christensen, J., Marotzke, J., Power, S., Rummukainen, M. and Zhou, T. (2013) Atlas of global and regional climate projections. In: Stocker, T.F., Qin, D., Plattner, G.-K., Tignor, M., Allen, S.K., Boschung, J., Nauels, A., Xia, Y., Bex, V. and Midgley, P.M. (Eds.) *Climate Change 2013: The Physical Science Basis. Contribution of Working Group 1 to the Fifth Assessment Report of the Intergovernmental Panel on Climate Change*. Cambridge: Cambridge University Press, pp. 1311–1394.

Oreskes, N. (2000) Why predict? Historical perspectives on prediction in Earth science. In: Sarewitz, D., Pielke, R.A. , Jr. and Byerly, R. , Jr. (Eds.) *Prediction: Science Decision Making and the Future of Nature*. Washington, D.C.: Island Press.

Pittman, J., Wittrock, V., Kulshreshtha, S. and Wheaton, E. (2011) Vulnerability to climate change in rural Saskatchewan: case study of the rural municipality of Rudy no. 284. *Journal of Rural Studies*, 27, 83–94.

Sauchyn, D. and Ilich, N. (2017) Nine hundred years of weekly streamflows: stochastic downscaling of ensemble tree-ring reconstructions. *Water Resources Research*, 53, 9266–9283. https://doi.org/10.1002/2017WR021585.

Sauchyn, D.J., Vanstone, J.R., St. Jacques, J.-M. and Sauchyn, R.D. (2015) Dendrohydrology in Western Canada and applications to water resource management. *Journal of Hydrology*, 529, 548–558.

Sauchyn, D., Velez Upegui, J.J., Masiokas, M., Ocampo, O., Cara, L. and Villalba, R. (2016) Exposure of rural communities to climate variability and change: case studies from Argentina, Colombia and Canada, chapter 2. In: Filho, W.L., et al. (Eds.) *Implementing Climate Change Adaptation in Cities and Communities, Climate Change Management*. Switzerland: Springer International Publishing. https://doi.org/10.1007/978-3-319-28591-7_2.

Sheffield, J., Camargo, S.J., Fu, R., Hu, Q., Jiang, X., Johnson, N., Karnauskas, K.B., Kim, S.T., Kinter, J., Kumar, S., Langenbrunner, B., Maloney, E., Mariotti, A., Meyerson, J.E., Neelin, J.D., Nigam, S., Pan, Z., Ruiz-Barradas, A., Seager, R., Serra, Y.L., Sun, D.-Z., Wang, C., Xie, S.-P., Yu, J.-Y., Zhang, T. and Zhao, M. (2013) North American climate in CMIP5 experiments. Part II: evaluation of historical simulations of intraseasonal to decadal variability. *Journal of Climate*, 26, 9247–9290.

Stewart, I., Cayan, D.R. and Dettinger, M.D. (2005) Changes toward earlier streamflow timing across western North America. *Journal of Climate*, 18, 1136–1155.

Sui, Y., Lang, X. and Jiang, D. (2014) Time of emergence of climate change signals over China under the RCP4.5 scenario. *Climatic Change*, 125, 265–276. https://doi.org/10.1007/s10584-014-1151-y.

St. Jacques, J.M., Sauchyn, D.J. and Zhao, Y. (2010) Northern Rocky Mountain streamflow records: global warming trends, human impacts or natural variability? *Geophysical Research Letters*, 37, L06407. https://doi.org/10.1029/2009GL042045.

Taylor, K.E., Stouffer, R.J. and Meehl, G.A. (2012) An overview of CMIP5 and the experiment design. *Bulletin of the American Meteorological Society*, 93, 485–498.

Whitfield, P.H., Moore, R.D., Fleming, S.W. and Zawadzki, A. (2010) Pacific decadal oscillation and the hydroclimatology of Western Canada—reviews and prospects. *Canadian Water Resources Journal*, 35, 1–28.

Wise, E.K. (2010) Spatiotemporal variability of the precipitation dipole transition zone in the western United States. *Geophysical Research Letters*, 37, L07706.

SUPPORTING INFORMATION

Additional supporting information may be found online in the Supporting Information section at the end of this article.

How to cite this article: Barrow EM, Sauchyn DJ. Uncertainty in climate projections and time of emergence of climate signals in the western Canadian Prairies. *Int J Climatol*. 2019;1–14. https://doi.org/10.1002/joc.6079